

Structural Studies Unravel the Active Conformation of Apo ROR $\gamma$ t Nuclear Receptor and a  
Common Inverse Agonism of Two Diverse Classes of ROR $\gamma$ t Inhibitors

Xiang Li<sup>1\*</sup>, Marie Anderson<sup>1</sup>, Delphine Collin<sup>1</sup>, Ingo Muegge<sup>1</sup>, John Wan<sup>1</sup>, Debra Brennan<sup>1</sup>,  
Stanley Kugler<sup>1</sup>, Donna Terenzio<sup>1</sup>, Charles Kennedy<sup>1</sup>, Siqi Lin<sup>1</sup>, Mark E. Labadia<sup>2</sup>, Brian  
Cook<sup>1</sup>, Robert Hughes<sup>1</sup>, and Neil A. Farrow<sup>1</sup>

From the <sup>1</sup>Department of Small Molecule Discovery Research, <sup>2</sup>Department of Immunology and  
Respiratory Diseases, Boehringer Ingelheim Pharmaceuticals, Inc., 900 Ridgebury Road, P.O.  
Box 368, Ridgefield, CT 06877-0368, USA

Running title: *Apo and ligand-bound ROR $\gamma$ t structures*

To whom correspondence should be addressed: Xiang Li, Department of Small Molecule  
Discovery Research, Boehringer Ingelheim Pharmaceuticals, Inc., 900 Ridgebury Road, P.O. Box  
368, Ridgefield, CT 06877-0368, USA. Tel: (203) 798-4198; Fax: (203) 837-4198; E-mail:  
xiang.li@boehringer-ingelheim.com

**Keywords:** Retinoid acid-related orphan receptor  $\gamma$ t (ROR $\gamma$ t), nuclear receptor, crystal structure,  
X-ray crystallography, nuclear magnetic resonance (NMR), ab initio calculations, protein drug  
interaction, drug discovery

## Abstract

The nuclear receptor retinoid acid-related orphan receptor  $\gamma$ t (ROR $\gamma$ t) is a master regulator of the Th17/IL-17 pathway that plays crucial roles in the pathogenesis of autoimmunity. ROR $\gamma$ t has recently emerged as a highly promising target for treatment of a number of autoimmune diseases. Through high-throughput screening we previously identified several classes of inverse agonists for ROR $\gamma$ t. Here, we report the crystal structures for the ligand binding domain of ROR $\gamma$ t in both apo and ligand-bound states. We show that apo ROR $\gamma$ t adopts an active conformation capable of recruiting coactivator peptides and present a detailed analysis of the structural determinants that stabilize helix 12 (H12) of ROR $\gamma$ t in the active state in the absence of a ligand. The structures of ligand-bound ROR $\gamma$ t reveal that binding of the inverse agonists disrupts critical interactions that stabilize H12. This destabilizing effect is supported by *ab initio* calculations and experimentally by a normalized crystallographic B-factor analysis. Of note, the H12 destabilization in the active state shifts

the conformational equilibrium of ROR $\gamma$ t toward an inactive state, which underlies the molecular mechanism of action for the inverse agonists reported here. Our findings highlight that nuclear receptor structure and function are dictated by a dynamic conformational equilibrium and that subtle changes in ligand structures can shift this equilibrium in opposite directions, leading to a functional switch from agonists to inverse agonists.

## Introduction

The Th17 lineage of T helper cells play essential roles in protective immunity against a variety of bacteria such as *Mycobacteria tuberculosis* and *Staphylococcus aureus* and pathogenic fungi such as *Candida albicans* (1). Individuals with genetic defects in Th17 pathway are susceptible to recurrent bacterial infections and often develop unrelenting chronic mucocutaneous candidiasis (CMC) (2,3). However, Th17 cells, which produce the eponymous IL-17A (often simply referred to as IL-17) and other proinflammatory cytokines including IL-17F, IL-21, IL-22 and

granulocyte-macrophage colony-stimulating factor (GM-CSF), are also potent inducers of multiple autoimmune diseases in animal models (4-8) and are strongly implicated by human genetic studies in the pathogenesis of most common human autoimmune diseases including psoriasis, psoriatic arthritis, Crohn's disease, ankylosing spondylitis, rheumatoid arthritis and multiple sclerosis (9-13). Given the prominent roles of the Th17/IL-17 pathway in autoimmunity, therapeutic interventions targeting this pathway have been intensely pursued. Two monoclonal antibodies (mAb) targeting IL-17A, secukinumab (Cosentyx) and ixekizumab (Taltz), have been approved recently for the treatment of moderate to severe plaque psoriasis. Secukinumab is also approved for psoriatic arthritis and ankylosing spondylitis (14). In Phase 3 clinical trials both secukinumab and ixekizumab have demonstrated remarkable efficacy for treatment of psoriasis with ~ 90% of patients achieving a 75% reduction in psoriasis area and severity index (PASI75) and ~ 40% achieving a PASI100 response with complete clearing of skin lesions (15). Similar efficacy has been achieved by brodalumab (Siliq), a mAb targeting the IL-17 receptor IL-17RA, which was recently approved by the US Food and Drug Administration to treat adults with moderate to severe plaque psoriasis (16). Other mAbs, such as guselkumab, tildrakizumab, risankizumab (BI 655066) and AMG 139, that target the p19 subunit of IL-23 – a critical cytokine for pathogenic Th17 lineage commitment and expansion, also show excellent efficacy for psoriasis (15). Collectively, the successes of these biologics have strongly validated clinically IL-17, IL-17R and IL-23 – all key players in the Th17 pathway – as valuable therapeutic targets for autoimmune diseases.

The nuclear receptor (NR) retinoid acid-related orphan receptor  $\gamma$ t (ROR $\gamma$ t) is a master transcription factor of Th17 cells, being both necessary and sufficient for IL-17 expression, and is essential in promoting Th17 cell differentiation while suppressing the Th1 program (17,18). ROR $\gamma$ t is also required for the production of IL-17 from other cell types

including  $\gamma\delta$  T cells, invariant natural killer T cells (iNKT) and Group 3 innate lymphoid cells (ILC), and is necessary for Th17 cells to produce other proinflammatory cytokines such as IL-22, GM-CSF and the IL-23R (19). Therefore small-molecule modulators against ROR $\gamma$ t are also a highly attractive therapeutic modality that has the potential for meaningful pharmacological differentiation from the specific anti-IL-17 or anti-IL-23 mAbs. Many small-molecule modulators of ROR $\gamma$ t have been reported in the literature in recent years, and two compounds have reached Phase-2 clinical trials for treatment of psoriasis (20-22).

There are 3 members in the ROR subfamily of human NRs: ROR $\alpha$  (RORA, NR1F1), ROR $\beta$  (RORB, NR1F2) and ROR $\gamma$  (RORC, NR1F3). The members of the subfamily share about 50% sequence identity in their ligand binding domains (LBD). Two isoforms of ROR $\gamma$  exist: the canonical ROR $\gamma$  (ROR $\gamma$ 1), and ROR $\gamma$ t (ROR $\gamma$ 2), which lacks the first 21 N-terminal amino acids due to alternative promoter usage. The ROR $\gamma$  isoform is expressed in most tissues and is involved in many physiological functions (23). ROR $\gamma$ t, on the other hand, is solely expressed in lymphoid lineage cells of the immune system, consistent with its essential roles in the development of lymph nodes as well as Th17 cells (23). Despite the word “orphan” in ROR $\gamma$ 's name, recent studies with sterol auxotroph cells have convincingly shown that sterol lipids, including certain cholesterol biosynthetic intermediates (CBI) and oxysterols, are physiological ligands for ROR $\gamma$  (24–26). An important link between lipid metabolism and regulation of Th17 pathogenicity was established recently by the discovery that CD5 antigen-like (CD5L) acts as a negative regulator that alters the balance of lipid saturation and directly affects the availability of sterol ligands for ROR $\gamma$ t (27).

Crystal structures of ROR $\gamma$  LBD in complex with hydroxycholesterols and various synthetic ligands have been reported (28-36). But to our knowledge no apo structure of ROR $\gamma$  LBD has yet been published. Here we report the crystal structures of ROR $\gamma$ t LBD in

both apo and ligand-bound states with two novel classes of synthetic ligands. The apo ROR $\gamma$ t structure adopts a predominantly active conformation, which is supported by the NMR experiments in solution. Density functional theory (DFT) calculations were used to elucidate the energetics of the structural determinants underlying the active conformation of ROR $\gamma$ t. A common theme for the structural mechanism of action of the two distinct classes of inverse agonists was revealed from analyses of the respective complex structures and normalized crystallographic B-factors. We emphasize that the dynamic conformational equilibrium is a fundamental attribute to understand NR structure and function. Indeed, subtle changes in ligand structures can shift the equilibrium in opposite directions and lead to a functional switch from an agonist to an inverse agonist.

## Results

*Production and Crystallization of SRC2-peptide Tethered ROR $\gamma$ t-LBD* – Structural studies of NRs are often carried out in the presence of carefully chosen cofactor peptides that bind and stabilize the receptors, as is the case in the first crystallographic study of the ROR $\gamma$ t-LBD (28). When examining the published crystal structure (PDB ID: 3L0L) we noticed that the C $\alpha$ –C $\alpha$  distance is only 8 Å between the first resolved N-terminal residue of the steroid receptor coactivator-2 (SRC2) peptide and the C-terminal residue (S507) of the ROR $\gamma$ t-LBD. Modeling suggested that it might be possible to covalently tether a SRC2 peptide to the C-terminus of ROR $\gamma$ t-LBD via a simple -GGG-linker. The tri-Glycine linker provides the maximal conformational flexibility to preserve the native interactions between the tethered partners with minimal interference. The tethered system is thermodynamically more stable than the untethered complex due to the reduction of macroscopic translational entropy through tethering (37,38). We therefore produced the 6His–ROR $\gamma$ t-LBD(260-507) – GGG–EKHKILHRLQDS (SRC2 peptide) construct and expressed it in *E. coli*. The chimeric protein expressed well in a soluble

form, and was straightforward to purify using standard affinity and size exclusion chromatography (see Experimental procedures). Similar approaches have been used in the study of PXR-LBD:SRC-1p complex (39), as well as MHC-II:peptide complexes and other protein-protein interactions (40,41). Without the complication of achieving the right stoichiometry for the peptide:receptor mixture, the apo crystals of ROR $\gamma$ t-LBD with tethered SRC2 peptide could be reproducibly obtained by sitting or hanging drop vapor diffusion at room temperature (see Experimental procedures). In most cases, co-structures with ligands were obtained by soaking of compounds into the apo ROR $\gamma$ t-LBD crystals. Very occasionally, co-crystallization, where a compound was pre-incubated with the protein solution prior to crystallization, was also used to solve a co-complex structure. This is the case for Compound 2 (Table 2), for which co-structures were obtained through both soaking and co-crystallization.

*The Apo ROR $\gamma$ t-LBD Structure and the Structural Determinants for Its Active Conformation* – The apo ROR $\gamma$ t-LBD structure was solved in the space group P4<sub>1</sub>2<sub>1</sub>2 with one polypeptide chain per asymmetric unit. The statistics for data collection and refinement is summarized in Table 1. The apo ROR $\gamma$ t-LBD structure is very similar to that of the 25-hydroxycholesterol (25-HC) bound ROR $\gamma$ t (28) (PDB ID: 3L0L), with r.m.s.d of backbone and all heavy atoms at 0.54 Å and 1.20 Å between the two structures, respectively (Figure 1). Similar to 25-HC bound ROR $\gamma$ t, the apo structure assumes an active conformation, with H12 as an integral part of the AF-2 surface that captures the SRC2 coactivator peptide (Figure 1A). The –GGG– linker residues are in a flexible loop conformation with weak electron densities and elevated B-factor values. There are no specific interactions between the glycine linker and the rest of the protein. Notably, the apo ROR $\gamma$ t contains a large ligand binding pocket, with a cavity volume of 940 Å<sup>3</sup> (Figure 1A). As is typical for nuclear receptors, the ligand

binding pocket is predominantly hydrophobic (575 Å<sup>3</sup>, 61% of total cavity volume). In contrast, the cavity volumes for hydrophilic, basic and acidic compositions are 161 Å<sup>3</sup> (17%), 178 Å<sup>3</sup> (19%) and 26 Å<sup>3</sup> (3%), respectively. Interestingly, almost the entire 25-HC can fit comfortably in the ligand binding pocket of apo ROR $\gamma$ t; only some adaptive sidechain movements from His323, Leu324 and M365 are required to accommodate the B-ring of 25-HC (Figure 1B). In fact the His323 sidechain conformation switch constitutes the largest structural difference between the apo and 25-HC bound ROR $\gamma$ t. It has been shown recently that a number of cholesterol precursors such as lanosterol and desmosterol, as well as oxysterols, are the natural endogenous ligands for ROR $\gamma$ t (24-26). Our structure of apo ROR $\gamma$ t suggests that the ligand binding pocket may be pre-formed to readily accommodate such ligands.

The question then arises as to how ROR $\gamma$ t keeps H12 in the active conformation and maintains a large cavity in its interior in the absence of a ligand. One key structural element is the His479-Tyr502-Phe506 triplet. Tyr502 and Phe506 reside on the same face of the two-turn H12, forming close interactions with His479 on H11 (Figure 1C). The most prominent of the interactions is the H-bond between the phenol of Tyr502 and the imidazole N<sup>ε2</sup> of His479. Here the N<sup>ε2</sup> of His479 acts most likely as an H-bond acceptor and thus His479 is in the neutral (uncharged) form. His479 also engages in an edge-to-face aromatic packing interaction with Phe506. Furthermore, a favorable aromatic ring packing exists between Tyr502 and Phe506. The sidechain rotamer of His479 is further stabilized through a water-mediated H-bond network linking its N<sup>δ1</sup> to the backbone carbonyl oxygen of Gln475. To more quantitatively assess the significance of these interactions, an *ab initio* calculation of the interaction energy among the sidechains of the HYF triplet was carried out using the DFT method (see Experimental procedures). The DFT calculation used the Truhlar hybrid meta

exchange-correlation functional M06-2X with a 6-32G\*\* basis set, which is well-suited for calculating non-covalent interactions such as H-bonding and  $\pi$ -stacking that are dominated by dispersion forces (42,43). The resulting interaction energy for the HYF triplet is -12.90 kCal/mol. This is a very significant energy which provides the anchoring force to stabilize H12 of ROR $\gamma$ t in the active conformation in the absence of a ligand. The HYF triplet is conserved among the  $\alpha/\beta/\gamma$  isoforms of the ROR subfamily, but is not found in any other NRs. For example, the corresponding residues in PPAR $\gamma$  are His449-Leu469-Tyr473 with no H-bonding among them. The interaction energy is only -3.00 kCal/mol when PPAR $\gamma$  is in the active conformation, and negligible when PPAR $\gamma$  is in the inactive conformation (interaction energies calculated using the same DFT method, with PPAR $\gamma$  coordinates from PDB ID: 1PRG. See Figure S1 in Supplemental material). Due to the lack of a stabilizing triplet in PPAR $\gamma$ , the H12 and indeed the entire ligand binding pocket of apo PPAR $\gamma$  exhibit significant conformational mobility as revealed by NMR (44) and fluorescence anisotropy studies (45). The crystal structure of apo PPAR $\gamma$  also showed elevated crystallographic B-factor values for the H12 and ligand binding pocket residues, and H12 was in fact captured in both active and inactive states (46).

There is another unique structural element in ROR, namely the H11' helix. Again H11' is present in all three isoforms of the ROR subfamily but not found in most of the other NRs. As illustrated in Figure 1D, H11' and H12 together bury 322 Å<sup>2</sup> of solvent accessible surface area, which is 29% of H12's total surface area. Therefore a notable helical packing interaction exists between H11' and H12. Helical packing in general is an important stabilizing force in protein folding and in protein-protein interactions (47,48). Here the H11'-H12 packing contributes to stabilize H12 in the active conformation. Interestingly H12 and the SRC2 peptide together bury 509 Å<sup>2</sup> of solvent accessible surface area (Figure 1D), which amounts to 46%



and 32% of total surface area for H12 and the SRC2 peptide, respectively, and underscores the critical role H12 plays in recruiting co-activators. In summary, ROR $\gamma$ t utilizes a unique HYF triplet to provide a significant interaction energy to anchor H12 in the active conformation, which is further stabilized by helical packing with a unique H11' element.

*ROR $\gamma$ t-LBD Is Capable of Recruiting Coactivator Peptide in the Absence of a Ligand* – A hallmark of a NR in the active state is its ability to recruit coactivators to initiate transcription. To investigate whether apo ROR $\gamma$ t is competent to bind coactivators, we carried out solution NMR studies using  $^{13}\text{C}/^{15}\text{N}$  labeled samples from a ROR $\gamma$ t(259-518) construct as well as the crystallography construct ROR $\gamma$ t(260-507)-G<sub>3</sub>-SRC2. The ROR $\gamma$ t(259-518) construct encompasses the entire ROR $\gamma$ t ligand binding domain, without C-terminal truncation beyond H12 and without tethering of a coactivator peptide. As shown in Figure 2, titration of the SRC2 peptide into the  $^{13}\text{C}/^{15}\text{N}$  labeled ROR $\gamma$ t(259-518) protein resulted in distinctive chemical shift perturbations to the backbone amide peaks in the  $^{15}\text{N}$ -TROSY spectra (Figure 2A) as well as to the methyl peaks in the  $^{13}\text{C}$ -HSQC spectra (Figure 2B) of ROR $\gamma$ t(259-518). These results clearly demonstrate that the native ROR $\gamma$ t-LBD in solution is capable of binding to a coactivator peptide, such as the SRC2 peptide used here, in the absence of a ligand. Furthermore, the backbone  $^{15}\text{N}$ -TROSY spectrum of the SRC2-bound ROR $\gamma$ t(259-518) bears strong resemblance to that of the ROR $\gamma$ t(260-507)-G<sub>3</sub>-SRC2 (Figure 2C). Some of the differences between the two spectra with proton chemical shift centered around 8 ppm in Figure 2C are likely due to the difference of C-terminal sequences after residue 507. The resemblance is even more striking for the methyl resonances in the  $^{13}\text{C}$ -HSQC spectra (Figure 2D, and compare with Figure 2B), with the perturbed methyl peaks from ROR $\gamma$ t(259-518) shifting to the exact positions of the corresponding methyl peaks from ROR $\gamma$ t(260-507)-G<sub>3</sub>-SRC2. Therefore the SRC2-tethered ROR $\gamma$ t-LBD largely

recapitulates the native ROR $\gamma$ t-LBD in the presence of the SRC2 peptide in solution. It should be noted from qualitative assessments of the NMR spectra that the native apo ROR $\gamma$ t-LBD exhibits more conformational flexibility in solution than the SRC2-tethered apo ROR $\gamma$ t-LBD. There is also evidence that the C-terminal residues beyond H12 (*i.e.* residues 508 – 518) in the native ROR $\gamma$ t-LBD are largely disordered both in solution and in crystal forms (see Footnotes).

*Binding Mode of Two Diverse Classes of ROR $\gamma$ t Inverse Agonists and the Structural Mechanism of Action (sMOA)* – Two classes of ROR $\gamma$ t inverse agonists were discovered through a High-Throughput Screening (HTS) campaign using a ROR $\gamma$ t gene reporter assay (Experimental procedures). Two representative compounds from the two classes are shown in Table 2. These compounds had sub- $\mu\text{M}$  binding affinity to ROR $\gamma$ t in a fluorescence polarization (FP) competition assay using a probe with similar potency in a cell-based ROR $\gamma$ t reporter gene assay. More importantly, these compounds also demonstrated Th17 primary cell activity, inhibiting the production of IL-17.

A 2.04 Å resolution co-complex structure of Compound **1** with ROR $\gamma$ t-LBD was obtained through soaking of the compound in the apo ROR $\gamma$ t crystals. As shown in Figure 3A, Compound **1** binds across the entire cavity of the ligand binding pocket, starting from one end with the pyridine nitrogen making a strong H-bond with Arg367, the urea carbonyl in the middle forming a water-mediated H-bond with the backbone carbonyl of Phe377, and the isobutylene moiety extending into a highly hydrophobic region lined with aliphatic and aromatic residues, and ending with the phenyl amide interacting with the critical HYF triplet. Most notably, the phenyl ring of Compound **1** protrudes into the His479-Tyr502 pair, disrupting the H-bond between them. His479 is forced to adopt a different sidechain conformation, which is stabilized through the formation of two new H-bonds with the amide linker of Compound **1** and the backbone

carbonyl of Leu475, respectively (Figure 3B). The two aromatic residues on H12, Tyr502 and Phe506, however, lose their close interactions with His479. In this case, the interaction energy of the HYF triplet is reduced to only -1.4 kCal/mol as calculated using the same DFT protocol, which amounts to a loss of 11.5 kCal/mol stabilizing energy for H12 compared to the apo structure. Therefore the disruption by Compound **1** of the critical H-bond between His479 and Tyr502, with a concurrent loss of the aromatic packing between His479 and Phe506, results in the severe destabilization of H12 in its active conformation.

Compound **2** is structurally very different from Compound **1**. To understand how Compound **2** binds to ROR $\gamma$ t and what is the structural basis for its mechanism of action, we also solved its co-complex structure with ROR $\gamma$ t-LBD. Both soaking and co-crystallization approaches were attempted, and both yielded co-structures that are highly similar to each other; therefore, only the structure from co-crystallization is reported here. Despite having completely unrelated chemical structures, Compounds **1** and **2** occupy essentially the same space in the ligand binding pocket of ROR $\gamma$ t (Figure 3C). The isobutyl group of Compound **2** aligns with the pyridyl ring of Compound **1**, although the former does not engage Arg367 in an H-bond. The methyl piperidine moiety of Compound **2** fills the same hydrophobic sub-pocket that accepts the isobutylene moiety of Compound **1**. A very similar water-mediated H-bond is observed between Compound **2** and the backbone carbonyl of Phe377. Most interestingly, the chlorobenzyl group of Compound **2** also intercalates into the His479-Tyr502 pair, forcing a sidechain conformation switch for His479 and breaking up the His479-Tyr502 H-bond (Figure 3D). The interaction energy of the HYF triplet is lost almost completely at -1.1 kCal/mol based on the DFT calculation. The loss of favorable interactions for His479 is partly compensated for by the formation of new H-bonds with the amide linker of Compound **2** and the backbone carbonyl of Leu475, in a way reminiscent of

the case with Compound **1**. It appears therefore that we have uncovered a common mechanism by which diverse chemical scaffolds may exert inverse agonist activities against ROR $\gamma$ t through direct disruption of the tightly interacting HYF triplet thereby destabilizing the active conformation of ROR $\gamma$ t.

*Differential B-Factor Analysis* – The crystallographic B-factor, also called atomic displacement parameter (ADP), is a measure of atomic displacement from its equilibrium or mean position, and captures structural flexibility as well as positional variations due to thermal vibrations. Not surprisingly B-factors have been widely exploited to probe protein flexibility (49), thermal stability (50), enzyme active sites (51), and, more recently, to provide an integrated description of protein dynamics by combining with order parameters derived from solution NMR studies (52). Likewise, we reasoned that the destabilization of ROR $\gamma$ t's H12 due to the binding of Compounds **1** and **2** should be manifested by elevated B-factors in the H12 region of the respective complex structures. Typically, B-factor analyses of proteins are performed to compare different regions of the same protein structure. Here, we want to compare B-factors in the same regions of the protein from two different structures. To allow for a meaningful comparison of B-factors between the H12 region of interest in the bound state and the corresponding apo state, we first introduce a modified B-factor:

$$B' = \frac{B - \langle B \rangle_{median}}{\langle B \rangle_{median}} \quad (1)$$

where  $\langle B \rangle_{median}$  is the median B-factor, calculated separately for backbone and sidechain atoms respectively.  $B'$  can be viewed as a normalized B-factor. It is not influenced by variation of overall B-factors between different crystals.  $B'$  is dimensionless. A negative (positive)  $B'$  value can be interpreted as indicative of higher (lower) rigidity and stability than the average of the structure. To identify regions of altered flexibility or stability in the compound-bound complex

versus the corresponding apo state, we examine:

$$B_{diff} = B'_{complex} - B'_{apo} \quad (2)$$

An atom with positive  $B_{diff}$  means it has elevated flexibility and is less stable compared to its apo state. Conversely, an atom with negative  $B_{diff}$  means it is further rigidified and more stable than in the apo state. In Figure 4, the  $B_{diff}$  values are visualized with color ramps from blue (negative) to white (0) to red (positive) for H11 and H12 of ROR $\gamma$ t in complex with Compound **1** (Figure 4A) and **2** (Figure 4B) respectively. As already suggested by the DFT calculations, the destabilization of H12 and the HYF triplet by the ligands is reflected in the  $B_{diff}$  plots by red colorations of H12.

In addition to showing how ligands can destabilize H12 we surmised that it should also be possible that ligands can further stabilize H12 in the active conformation. To this end, we studied Compound **3**, which was synthesized as an analog of Compound **1** following a typical structure-activity-relationship (SAR) optimization strategy. Compound **3** is structurally very similar to Compound **1** except having an ether linker in place of an amide in Compound **1**. Compound **3** showed good binding to ROR $\gamma$ t (FP  $K_i$  = 0.19  $\mu$ M), but surprisingly did not register an inhibitory activity in the reporter gene assay ( $IC_{50}$  > 3.3  $\mu$ M). To understand its unexpected lack of inverse agonist activity we solved a 2.34 Å resolution co-complex structure of Compound **3** with ROR $\gamma$ t-LBD through soaking of the compound in the apo ROR $\gamma$ t crystals (Figure 3E). Surprisingly, Compound **3** does not disrupt the tightly interacting HYF triplet. Instead the phenyl ether of Compound **3** points towards Trp317 and forms a tightly packed aromatic cluster with the HYF triplet and Trp317 together, thereby further stabilizing ROR $\gamma$ t in the active conformation (Figure 3F). This stabilization effect is confirmed by the differential B-factor analysis shown in Figure 4C. Since the inverse agonist activities of Compound **1** and **2** are due to their destabilization effect on the active

receptor conformation of ROR $\gamma$ t as discussed above, it is expected that stabilization of the active conformation by Compound **3** would elicit the opposite effect on the receptor. In other words, Compound **3** should be an agonist of ROR $\gamma$ t. A fluorescence polarization (FP) based coactivator recruitment assay using a fluorescein labeled coactivator peptide (D22) containing the LXXLL motif was developed to test this. As shown in Figure 5, Compound **3** indeed behaves as an agonist by enhancing the recruitment of D22 with an  $EC_{50}$  of 0.54  $\mu$ M.

## Discussion

Nuclear receptors are ligand-regulated transcription factors that orchestrate the assembly of co-regulatory complexes (coactivators and corepressors) to modulate transcription through chromatin remodeling activities (53). The role of a high affinity endogenous ligand is “classically” viewed as a trigger of a molecular switch whereby the binding of the ligand induces a conformational change involving H12 that switches the receptor from an inactive or repressed state to an active state competent for recruitment of coactivators and subsequent initiation of transcription (54). This conceptually appealing but overly simplistic view of NR activation is still frequently cited in the literature, even though mounting evidence has accumulated revealing NR proteins are highly dynamic and versatile. For instance REV-ERB $\alpha$  and REV-ERB $\beta$  do not even have a H12 and use Heme as a ligand (55,56); NR activities are spatially and temporally regulated (57), and involve multiple structural elements with specific higher-order structures at play (58,59). NRs are also known to be regulated by ligand-independent mechanisms such as post-translational modifications (60,61). For example, ROR $\gamma$ t has been shown to be modulated by both acetylation (62) and ubiquitination (63) with direct functional effects on Th17 biology. In this study we showed that the apo ROR $\gamma$ t LBD can adopt an active conformation with the capability to recruit a coactivator peptide. We believe that this active conformation is not influenced by

the triple-glycine linker since these glycines do not make any specific contacts with the rest of the protein in the crystal structure and are highly flexible with very weak electron densities and high B-factors. In full support of this notion, our solution NMR studies with the ROR $\gamma$ t(259-518) construct demonstrated that the non-tethered native ROR $\gamma$ t LBD is capable of directly binding to the SRC2 coactivator peptide in the absence of a ligand, and the NMR spectra of SRC2-bound ROR $\gamma$ t LBD closely resemble those of the SRC2-tethered ROR $\gamma$ t-LBD, suggesting both having similar conformations in solution.

A number of NRs, such as ESRRG, NGFIB, NURR1 and LRH-1, are capable of adopting active conformations independent of ligands (64). The crystal structure of apo LRH-1 (65) in particular shows an active conformation with a voluminous but empty cavity (820 Å) in the ligand binding pocket, very similar to the case with apo ROR $\gamma$ t revealed here. The specific structural elements stabilizing apo LRH-1 in the active conformation have been attributed to an extended H2 that acts as an extra layer with optimal helical packing against H3 to hold AF2 helices, including H12, in the activated state (65). In this study we have carried out detailed structural and computational analyses to demonstrate that the tightly interacting His479-Tyr502-Phe506 triplet is the primary structural element responsible for anchoring ROR $\gamma$ t in the active conformation, which is further strengthened by additional helical packing with the extra H11' helix. Both the HYF triplet and the H11' are structural features unique to the ROR subfamily of NRs.

Proteins exist not in a single fixed state but rather as a dynamic ensemble in the biologically relevant environment. The apo crystal structure of ROR $\gamma$ t LBD reported here is only a snapshot of a continuum of conformations sampled by ROR $\gamma$ t in solution. The snapshot revealed by crystallography represents a low energy state having a dominant population. Under physiological conditions ROR $\gamma$ t should be able to also

sample other lower population (higher energy) states, including inactive ones. In fact our NMR studies with the ROR $\gamma$ t(259-518) construct have confirmed that ROR $\gamma$ t can indeed bind directly to a corepressor peptide derived from the silencing mediator of retinoid and thyroid hormone receptors-2 (SMRT2) in solution in the absence of a ligand (Figure S2 in Supplemental material). Therefore we have shown that ROR $\gamma$ t has the conformational elasticity to bind either a coactivator (active conformation) or a corepressor (inactive conformation) in solution independent of ligands. It would be reasonable to posit that in general the presence of ligands or coregulators can alter the populations of various distinct states an NR may assume and shift the conformational equilibrium toward further activation or inactivation of the receptor. Under this dynamic equilibrium paradigm of NR modulation, the abundance of specific ligands, coactivators or corepressors would dictate the activation state of an NR in a particular cellular context.

The structural mechanism of action (sMOA) revealed by the crystallographic studies of the two novel classes of ROR $\gamma$ t inverse agonists dovetails with the dynamic equilibrium paradigm. Despite their high structural diversity, the two classes of inverse agonists share a common sMOA: they both disrupt the critical HYF triplet anchor thereby destabilizing the active conformation of H12 and shifting ROR $\gamma$ t towards inactivation. Conversely, an agonist of ROR $\gamma$ t should do the opposite. This is the case with Compound **3**, which forms an extended aromatic cluster together with the HYF triplet and further stabilizes H12 in the active conformation. The dynamic picture of H12 mobility and stability in response to ligand binding is supported by the differential B-Factor analysis as well as the *ab initio* calculations of the interaction energies employed in this study. Recently, cholesterol biosynthetic intermediates (CBIs) have been identified as natural ligands for ROR $\gamma$ t. We believe that these endogenous ligands work similarly to Compound **3** in that they also bind and further stabilize the active



conformation of ROR $\gamma$ t. Under physiological conditions the actions of endogenous ligands are likely necessary to achieve sustained activation of ROR $\gamma$ t due to other factors that can tilt the conformational equilibrium of the receptor towards repressed states.

Finally, it is interesting to note that subtle changes in the ligand structure can result in diametrically opposite functional responses of a nuclear receptor, as demonstrated by the two structurally very similar urea Compounds **1** and **3** reported here. This phenomenon can be understood most naturally from examining the dynamic equilibrium of receptor states, as Compounds **1** and **3** shift the conformational equilibrium of ROR $\gamma$ t in opposite directions. Similar results have been reported by Rene *et al.* (35) who showed a class of benzylsulfonamides as full inverse agonists of ROR $\gamma$ t with phenylsulfonamide analogs showing agonistic activities. The underlying sMOA described by the Genentech group is identical to what we have observed here, in that the phenylsulfonamides stabilize the active conformation of ROR $\gamma$ t while the benzylsulfonamides destabilize it. The subtleties that minimal variation of ligand structures can lead to dramatically different functional activities are not limited to NRs, but are in fact well-known in the GPCR field (66). Complex dynamic states are involved in the ligand regulation as well as signal transduction of GPCRs (67,68). The dynamic equilibrium paradigm appears to be a unifying framework applicable for understanding the subtle structure-activity relationships often encountered in receptor drug discovery.

### **Experimental procedures**

*Cloning, Expression and Purification* – Constructs for 6His-Thr-ROR $\gamma$ t(260-507)-GGG-SRC2 and 6His-Thr-ROR $\gamma$ t(259-518) were cloned into pET41a(+) vectors. The proteins were expressed in *E. coli*, strain BL21(DE3). Cell cultures were grown in TB media under kanamycin control, at 37°C until the optical absorbance at 600 nm reached 1.0. Temperature was then reduced to 18°C and expression induced with 0.5 mM isopropyl 1-

thio- $\beta$ -D-galactopyranoside (IPTG). The  $^{13}\text{C}/^{15}\text{N}$  labeled samples were expressed in  $^{13}\text{C}/^{15}\text{N}$ -enriched Bioexpress cell growth media (Cambridge Isotope Laboratories, Inc., Catalog No.: CGM-1000-CN). Cells were lysed in lysis buffer (20 mM Tris, pH 8.0, 150 mM NaCl, 0.5% CHAPS, 2 mM  $\beta$ -mercaptoethanol, 10% glycerol, 2 tablets/50 mL protease inhibitors (Roche Catalog No 12483700), 10 units/mL benzonase nuclease (Sigma Catalog No. E1014), and 0.1 mg/mL Lysozyme). After clarification by centrifugation at 4 °C, the soluble lysate was loaded onto a His-Trap column pre-equilibrated with Ni-Eq. buffer (20 mM Tris, pH 8.0, 150 mM NaCl, 2 mM  $\beta$ -mercaptoethanol, 10% glycerol, 0.05% CHAPS) and the protein eluted out with elution buffer (20 mM Tris, pH 8.0, 150 mM NaCl, 2 mM  $\beta$ -mercaptoethanol, 10% glycerol, 0.05% CHAPS and 500 mM imidazole). The eluted protein was further purified by size-exclusion chromatography on a Superdex 75 column. Finally the pure ROR $\gamma$ t protein was dialyzed into the storage buffer (25 mM HEPES, pH 7.0, 150 mM NaCl, 2 mM DTT) and concentrated to 9 mg/mL prior to crystallization. For NMR experiments,  $^{13}\text{C}/^{15}\text{N}$  labeled protein samples were purified similarly, and exchanged into the final NMR buffer (see below) and concentrated to 0.22 mM.

*Crystallization, Data Collection, and Structure Determination* – Initial screens of crystallization conditions were carried out with Crystal Screens I and II from Hampton Research, and NR-LBD HT-96 screening kit from Molecular Dimensions (MD1-34), using sitting drop vapor diffusion on a Mosquito instrument at 20 °C. Drops containing 0.1  $\mu\text{L}$  protein mixed with 0.1  $\mu\text{L}$  well solution were equilibrated against 80  $\mu\text{L}$  well solution. Follow-up optimizations were performed manually using hanging drop vapor diffusion with drops containing 1  $\mu\text{L}$  protein mixed with 1  $\mu\text{L}$  well solution equilibrated against 500  $\mu\text{L}$  well solution. Diffraction-quality apo or ligand bound ROR $\gamma$ t crystals were obtained with 2 – 8% (w/v) PEG4000, 0.6 M NaCl and 0.1 M

PIPES, pH 7.0. Crystals were flash frozen in liquid nitrogen with cryoprotectant prepared using the corresponding reservoir condition supplemented with 20% glycerol. Protein:ligand co-crystals were obtained either from soaking of the compound into apo ROR $\gamma$ t crystals, or from co-crystallization of the pre-formed protein:ligand complex solution. For co-crystallization, a compound was added to the protein stock solution with a protein:ligand molar ratio of about 1:5. The complex solution was incubated at room temperature for 40 minutes and then centrifuged at 14000 rpm for 35 minutes prior to crystallization experiments. For soaking experiments, 3 mM compound prepared in DMSO stock solution was added in a drop containing the apo ROR $\gamma$ t crystals and soaked at room temperature for 6 hours. The soaked crystals were then flash frozen in liquid nitrogen using the crystallization solution supplemented with 25% PEG400 as a cryoprotectant. X-ray diffraction data were collected at beamlines X06SA, or X06DA (for co-crystals with Compound **1**) of the Swiss Light Source using Pilatus 6M and 2M-F detectors, respectively. Diffraction data were processed using either d\*TREK or XDS (69,70). The initial structure was determined by molecular replacement with Phaser (71) as implemented in the PHENIX software suite (72) using the structure of ROR $\gamma$ t LBD in complex with 22(R)-hydroxycholesterol (PDB ID: 3L0J) as a search model. Ligand geometry restraints were generated using Corina (Molecular Networks GmbH). Multiple rounds of positional and isotropic B-factor refinement using phenix.refine followed by manual rebuilding using Coot (73) were carried out for each structure. The quality of the final model was evaluated using MolProbity (74). Structural figures were generated using PyMOL (Schrödinger, LLC).

*NMR Spectroscopy* – All NMR data were acquired at 30° C on an 800-MHz Bruker AvanceIII spectrometer equipped with a triple resonance ( $^1\text{H}/^{13}\text{C}/^{15}\text{N}$ ) cryoprobe. 0.22 mM samples of uniformly  $^{13}\text{C}/^{15}\text{N}$  labeled ROR $\gamma$ t(259-518) or ROR $\gamma$ t(260-507)-G<sub>3</sub>-

SRC2 in the same buffer containing 25 mM deuterated HEPES, pH 7.0, 150 mM NaCl, 2 mM DTT, with 10% D<sub>2</sub>O/90% H<sub>2</sub>O were used in the NMR experiments. Each NMR sample had a volume of 140  $\mu\text{L}$  using 2.5 mm Bruker Match tubes. For the titration experiments, SRC2 peptide was added to the ROR $\gamma$ t(259-518) sample with a final total peptide concentration of 0.4 mM. The  $^{15}\text{N}$  TROSY and  $^{13}\text{C}$  HSQC experiments were carried out as described in the literature (75-77).

*Fluorescence Polarization Competitive Binding Assays* – The fluorescence polarization (FP) measurements were conducted using an Envision plate reader (Perkin Elmer) using the ROR $\gamma$ t-SRC2 construct produced in-house (see above), and a fluorescent TAMRA (Thermo Fisher Scientific Inc.) probe synthesized with an in-house compound binding to ROR $\gamma$ t. Compound was diluted in assay buffer (20 mM Tris, pH7.5, 150 mM NaCl and 0.05% CHAPS) and 10  $\mu\text{L}$  of 20  $\mu\text{M}$  compound was mixed with 10  $\mu\text{L}$  of 2  $\mu\text{M}$  ROR $\gamma$ t-SRC2 in the same buffer and incubated for 30 minutes at room temperature. The TAMRA probe was then added to the mixture at a final concentration of 15 nM. After 30 minutes incubation at room temperature, the FP signal was measured (excitation wavelength 531 nm; emission wavelength 595 nm) and the  $K_d$  values were determined as described (78).

*ROR $\gamma$ t-Gal4 Reporter Gene Assay* – HEK293T cells were co-transfected with a plasmid pBIND containing the chimera of the DNA binding domain of the yeast Gal4 protein and the ligand binding domain of human ROR $\gamma$ t (Gal4DBD-hROR $\gamma$ t LBD), along with the luciferase reporter plasmid pGL4.31 (luc2P/GAL4UAS/Hygro, Promega). The positive control was co-transiently transfected with both plasmids, and the negative control had only the pGL4.31 promoter sequence. Assays were assembled in 384 well Greiner plates where transiently transfected cells and test compound at varying concentrations were incubated at 37°C and 5% CO<sub>2</sub> for 20-24 hours. The next day, assay

plates were taken out and equilibrated at room temperature for 20-30 minutes. Bright-Glo<sup>TM</sup> Luciferase Assay System (Promega) was used to detect luciferase production. After addition of Bright Glo detection reagent, the plates were incubated at room temperature for 20 minutes. The plates were read on an Envision plate reader to measure luminescence signal. The RLU signal was converted to percent of control (POC) value relative to control and blank wells.

**IL-17 Production in Th17 Primary Cell Assay** – Frozen CD4<sup>+</sup> T cells (AllCells) were thawed and resuspended in X-VIVO media (Lonza) at a cell density of  $1 \times 10^6$  cells/mL. Skewing cytokines were added to media at the final concentrations of 30 ng/mL IL-23, 10 ng/mL IL-1 $\beta$ , 10 ng/mL IL-6, 2 ng/mL IL-2, 4 ng/mL TGF $\beta$ 1, 5  $\mu$ g/mL IL-4 and 5  $\mu$ g/mL IFN $\gamma$ , and mixed with activated beads (Miltenyi Biotec Catalog No. 130-091-441) at 1 bead/cell. The cells were incubated under the stimulatory conditions for 72 hours at 37 °C. Skewed cells were spun and resuspended in Iscove's media (Invitrogen Catalog No. 12440) with a cell density of  $1.11 \times 10^6$  cells/mL. Cells were seeded at 90  $\mu$ L/well into Corning black/clear TC treated plates (Corning Catalog No. 3603) to give 100,000 cells per well. 10  $\mu$ L of media diluted compounds was added and plates incubated for 2 hours at 37°C and 5% CO<sub>2</sub>. 50  $\mu$ L of cytokine/bead mixture was added to all wells except blank wells, which received media only. Cell plates were incubated at 37°C and 5% CO<sub>2</sub> for 48 hours. Afterwards, plates were spun and 50  $\mu$ L supernatant from each well was collected and transferred to MSD Vplex IL-17A assay plate (Meso Scale Diagnostics, LLC) for detection of IL-17 expression, following manufacturer's protocol. IC<sub>50</sub> values were obtained by fitting 10 point concentration response data to a four-parameter logistic equation in ActivityBase (ID Business Solutions Ltd).

**Coactivator Recruitment Assay** – A fluorescence polarization (FP) based assay was developed for coactivator recruitment. The fluorescence polarization measurements

were conducted on an Envision (Perkin Elmer) using a ROR $\gamma$ t-GST construct produced in-house. The probe is a Fluorescein labeled coactivator peptide (D22) from Invitrogen containing the LXXLL motif, and optimized for binding to ROR $\gamma$ t ligand binding domain. 10  $\mu$ L of compounds diluted in 20 mM Tris, pH 7.5, 150 mM NaCl and 0.05% CHAPS were mixed to 10  $\mu$ L of 2  $\mu$ M ROR $\gamma$ t-GST in the same buffer and incubated for 30 minutes at room temperature. The fluorescein D22 probe was then added to the mixture at a final concentration of 15 nM. After 30 minutes incubation at room temperature, the FP signal was measured (excitation wavelength 480 nm; emission wavelength 535 nm).

**DFT Calculation** – Interaction energies between His479, Tyr502, and Phe506 of ROR $\gamma$ t LBD were calculated using the Density Functional Theory (DFT) routine implemented in Jaguar (79). A hybrid functional for non-covalent complexation energies, M06-2X (80), was applied together with a 6-31G\*\* basis set to calculate DFT energies. A self-consistent reaction field method using a Poisson Boltzmann solver (81) was applied as continuum solvation model with a dielectric constant of  $\epsilon=4$ . Interaction energies were calculated as the difference between the DFT energy of the residue triplet with atomic coordinates of His479, Tyr502, and Phe506 taken from the crystal structures reported here and three DFT energies associated with the individual residues calculated separately. To preserve the coordinates found in the crystal structures, only single point energies were calculated. The interaction energies for corresponding PPAR $\gamma$  residues were calculated based on the same DFT method, with PPAR $\gamma$  coordinates taken from PDB ID: 1PRG.

**Conflict of interest** – The authors declare no conflicts of financial interest with the contents of this article.

**Author contributions** – XL designed the X-ray construct, performed the NMR experiments, crystallized the apo ROR $\gamma$ t,

solved and analyzed all the X-ray structures including the B-factor analysis, and wrote the manuscript. MA carried out crystallization of ROR $\gamma$ t:ligand complexes. DC designed FP binding and coactivator recruitment assays and analyzed data. IM performed all the DFT calculations and contributed to the production of the manuscript. NAF contributed to protein and structural strategies and production of the manuscript. BK and RH designed ROR $\gamma$ t ligands used in this study and contributed to the interpretation of the studies. DB

contributed to protein expression and purification. JW carried out protein purification. MEL designed the ROR $\gamma$ t reporter assay and Th17 T cell assay. SL and CK developed and executed the ROR $\gamma$ t reporter gene assay for HTS campaign. SK and DT conducted the reporter gene assay and the Th17 cellular assay to support SAR optimization.

## References:

1. Korn, T., Bettelli, E., Oukka, M., and Kuchroo, V. K. (2009) IL-17 and Th17 Cells. *Annu Rev Immunol* **27**, 485-517
2. Glocker, E., and Grimbacher, B. (2010) Chronic mucocutaneous candidiasis and congenital susceptibility to Candida. *Curr Opin Allergy Clin Immunol* **10**, 542-550
3. Glocker, E. O., and Grimbacher, B. (2011) Mucosal antifungal defence: IL-17 signalling takes centre stage. *Immunol Cell Biol* **89**, 823-825
4. Langrish, C. L., Chen, Y., Blumenschein, W. M., Mattson, J., Basham, B., Sedgwick, J. D., McClanahan, T., Kastelein, R. A., and Cua, D. J. (2005) IL-23 drives a pathogenic T cell population that induces autoimmune inflammation. *J Exp Med* **201**, 233-240
5. Cua, D. J., Sherlock, J., Chen, Y., Murphy, C. A., Joyce, B., Seymour, B., Lucian, L., To, W., Kwan, S., Churakova, T., Zurawski, S., Wiekowski, M., Lira, S. A., Gorman, D., Kastelein, R. A., and Sedgwick, J. D. (2003) Interleukin-23 rather than interleukin-12 is the critical cytokine for autoimmune inflammation of the brain. *Nature* **421**, 744-748
6. Lubberts, E., Koenders, M. I., Oppers-Walgreen, B., van den Bersselaar, L., Coenen-de Roo, C. J., Joosten, L. A., and van den Berg, W. B. (2004) Treatment with a neutralizing anti-murine interleukin-17 antibody after the onset of collagen-induced arthritis reduces joint inflammation, cartilage destruction, and bone erosion. *Arthritis Rheum* **50**, 650-659
7. Sarkar, S., and Fox, D. A. (2010) Targeting IL-17 and Th17 cells in rheumatoid arthritis. *Rheum Dis Clin North Am* **36**, 345-366
8. Sherlock, J. P., Joyce-Shaikh, B., Turner, S. P., Chao, C. C., Sathe, M., Grein, J., Gorman, D. M., Bowman, E. P., McClanahan, T. K., Yearley, J. H., Eberl, G., Buckley, C. D., Kastelein, R. A., Pierce, R. H., Laface, D. M., and Cua, D. J. (2012) IL-23 induces spondyloarthritis by acting on ROR-gammat+ CD3+CD4-CD8- enthesal resident T cells. *Nat. Med* **18**, 1069-1076
9. Duerr, R. H., Taylor, K. D., Brant, S. R., Rioux, J. D., Silverberg, M. S., Daly, M. J., Steinhardt, A. H., Abraham, C., Regueiro, M., Griffiths, A., Dassopoulos, T., Bitton, A., Yang, H., Targan, S., Datta, L. W., Kistner, E. O., Schumm, L. P., Lee, A. T., Gregersen, P. K., Barmada, M. M., Rotter, J. I., Nicolae, D. L., and Cho, J. H. (2006) A genome-wide association study identifies IL23R as an inflammatory bowel disease gene. *Science* **314**, 1461-1463
10. Liu, Y., Helms, C., Liao, W., Zaba, L. C., Duan, S., Gardner, J., Wise, C., Miner, A., Malloy, M. J., Pullinger, C. R., Kane, J. P., Saccone, S., Worthington, J., Bruce, I., Kwok, P. Y., Menter, A., Krueger, J., Barton, A., Saccone, N. L., and Bowcock, A. M. (2008) A genome-wide association study of psoriasis and psoriatic arthritis identifies new disease loci. *PLoS Genet* **4**, e1000041



11. Lock, C., Hermans, G., Pedotti, R., Brendolan, A., Schadt, E., Garren, H., Langer-Gould, A., Strober, S., Cannella, B., Allard, J., Klonowski, P., Austin, A., Lad, N., Kaminski, N., Galli, S. J., Oksenberg, J. R., Raine, C. S., Heller, R., and Steinman, L. (2002) Gene-microarray analysis of multiple sclerosis lesions yields new targets validated in autoimmune encephalomyelitis. *Nat Med* **8**, 500-508
12. Australo-Anglo-American Spondyloarthritis, C., Reveille, J. D., Sims, A. M., Danoy, P., Evans, D. M., Leo, P., Pointon, J. J., Jin, R., Zhou, X., Bradbury, L. A., Appleton, L. H., Davis, J. C., Diekmann, L., Doan, T., Dowling, A., Duan, R., Duncan, E. L., Farrar, C., Hadler, J., Harvey, D., Karaderi, T., Mogg, R., Pomeroy, E., Pryce, K., Taylor, J., Savage, L., Deloukas, P., Kumanduri, V., Peltonen, L., Ring, S. M., Whittaker, P., Glazov, E., Thomas, G. P., Maksymowycz, W. P., Inman, R. D., Ward, M. M., Stone, M. A., Weisman, M. H., Wordsworth, B. P., and Brown, M. A. (2010) Genome-wide association study of ankylosing spondylitis identifies non-MHC susceptibility loci. *Nat Genet* **42**, 123-127
13. Miossec, P., and Kolls, J. K. (2012) Targeting IL-17 and TH17 cells in chronic inflammation. *Nat Rev Drug Discov* **11**, 763-776
14. Burkett, P. R., and Kuchroo, V. K. (2016) IL-17 Blockade in Psoriasis. *Cell* **167**, 1669
15. Patel, D. D., and Kuchroo, V. K. (2015) Th17 Cell Pathway in Human Immunity: Lessons from Genetics and Therapeutic Interventions. *Immunity* **43**, 1040-1051
16. Attia, A., Abushouk, A. I., Ahmed, H., Gadelkarim, M., Elgebaly, A., Hassan, Z., Abdel-Daim, M. M., and Negida, A. (2017) Safety and Efficacy of Brodalumab for Moderate-to-Severe Plaque Psoriasis: A Systematic Review and Meta-Analysis. *Clin Drug Investig*
17. Ivanov, I., McKenzie, B. S., Zhou, L., Tadokoro, C. E., Lepelley, A., Lafaille, J. J., Cua, D. J., and Littman, D. R. (2006) The orphan nuclear receptor ROR $\gamma$ t directs the differentiation program of proinflammatory IL-17+ T helper cells. *Cell* **126**, 1121-1133
18. Manel, N., Unutmaz, D., and Littman, D. R. (2008) The differentiation of human T(H)-17 cells requires transforming growth factor-beta and induction of the nuclear receptor ROR $\gamma$ t. *Nat Immunol* **9**, 641-649
19. Gaffen, S. L., Jain, R., Garg, A. V., and Cua, D. J. (2014) The IL-23-IL-17 immune axis: from mechanisms to therapeutic testing. *Nat Rev Immunol* **14**, 585-600
20. Fauber, B. P., and Magnuson, S. (2014) Modulators of the nuclear receptor retinoic acid receptor-related orphan receptor-gamma (ROR $\gamma$  or RORc). *J. Med. Chem* **57**, 5871-5892
21. Cyr, P., Bronner, S. M., and Crawford, J. J. (2016) Recent progress on nuclear receptor ROR $\gamma$  modulators. *Bioorg Med Chem Lett* **26**, 4387-4393
22. Bronner, S. M., Zbieg, J. R., and Crawford, J. J. (2017) ROR $\gamma$  antagonists and inverse agonists: a patent review. *Expert Opin Ther Pat* **27**, 101-112
23. Jetten, A. M. (2009) Retinoid-related orphan receptors (RORs): critical roles in development, immunity, circadian rhythm, and cellular metabolism. *Nucl Recept Signal* **7**, e003
24. Hu, X., Wang, Y., Hao, L. Y., Liu, X., Lesch, C. A., Sanchez, B. M., Wendling, J. M., Morgan, R. W., Aicher, T. D., Carter, L. L., Toogood, P. L., and Glick, G. D. (2015) Sterol metabolism controls T(H)17 differentiation by generating endogenous ROR $\gamma$  agonists. *Nat Chem Biol* **11**, 141-147
25. Santori, F. R., Huang, P., van de Pavert, S. A., Douglass, E. F., Jr., Leaver, D. J., Haubrich, B. A., Keber, R., Lorbek, G., Konijn, T., Rosales, B. N., Rozman, D., Horvat, S., Rahier, A., Mebius, R. E., Rastinejad, F., Nes, W. D., and Littman, D. R. (2015) Identification of natural ROR $\gamma$  ligands that regulate the development of lymphoid cells. *Cell Metab* **21**, 286-297
26. Soroosh, P., Wu, J., Xue, X., Song, J., Sutton, S. W., Sablad, M., Yu, J., Nelen, M. I., Liu, X., Castro, G., Luna, R., Crawford, S., Banie, H., Dandridge, R. A., Deng, X., Bittner, A.,

- Kuei, C., Tootoonchi, M., Rozenkrants, N., Herman, K., Gao, J., Yang, X. V., Sachen, K., Ngo, K., Fung-Leung, W. P., Nguyen, S., de Leon-Tabaldo, A., Blevitt, J., Zhang, Y., Cummings, M. D., Rao, T., Mani, N. S., Liu, C., McKinnon, M., Milla, M. E., Fourie, A. M., and Sun, S. (2014) Oxysterols are agonist ligands of ROR $\gamma$  and drive Th17 cell differentiation. *Proc Natl Acad Sci U S A* **111**, 12163-12168
27. Wang, C., Yosef, N., Gaublot, J., Wu, C., Lee, Y., Clish, C. B., Kaminski, J., Xiao, S., Meyer Zu Horste, G., Pawlak, M., Kishi, Y., Joller, N., Karwacz, K., Zhu, C., Ordovas-Montanes, M., Madi, A., Wortman, I., Miyazaki, T., Sobel, R. A., Park, H., Regev, A., and Kuchroo, V. K. (2015) CD5L/AIM Regulates Lipid Biosynthesis and Restrains Th17 Cell Pathogenicity. *Cell* **163**, 1413-1427
28. Jin, L., Martynowski, D., Zheng, S., Wada, T., Xie, W., and Li, Y. (2010) Structural basis for hydroxycholesterols as natural ligands of orphan nuclear receptor ROR $\gamma$ . *Mol Endocrinol* **24**, 923-929
29. Fujita-Sato, S., Ito, S., Isobe, T., Ohyama, T., Wakabayashi, K., Morishita, K., Ando, O., and Isono, F. (2011) Structural basis of digoxin that antagonizes ROR $\gamma$  receptor activity and suppresses Th17 cell differentiation and interleukin (IL)-17 production. *J Biol Chem* **286**, 31409-31417
30. Fauber, B. P., de Leon Boenig, G., Burton, B., Eidenschenk, C., Everett, C., Gobbi, A., Hymowitz, S. G., Johnson, A. R., Liimatta, M., Lockey, P., Norman, M., Ouyang, W., Rene, O., and Wong, H. (2013) Structure-based design of substituted hexafluoroisopropanol-arylsulfonamides as modulators of ROR $\gamma$ . *Bioorg Med Chem Lett* **23**, 6604-6609
31. Muegge, I., Collin, D., Cook, B., Hill-Drzewi, M., Horan, J., Kugler, S., Labadia, M., Li, X., Smith, L., and Zhang, Y. (2015) Discovery of 1,3-dihydro-2,1,3-benzothiadiazole 2,2-dioxide analogs as new ROR $\gamma$  modulators. *Bioorg Med Chem Lett* **25**, 1892-1895
32. Enyedy, I. J., Powell, N. A., Caravella, J., van Vloten, K., Chao, J., Banerjee, D., Marcotte, D., Silvian, L., McKenzie, A., Hong, V. S., and Fontenot, J. D. (2016) Discovery of biaryls as ROR $\gamma$  inverse agonists by using structure-based design. *Bioorg Med Chem Lett* **26**, 2459-2463
33. Hirata, K., Kotoku, M., Seki, N., Maeba, T., Maeda, K., Hirashima, S., Sakai, T., Obika, S., Hori, A., Hase, Y., Yamaguchi, T., Katsuda, Y., Hata, T., Miyagawa, N., Arita, K., Nomura, Y., Asahina, K., Aratsu, Y., Kamada, M., Adachi, T., Noguchi, M., Doi, S., Crowe, P., Bradley, E., Steensma, R., Tao, H., Fenn, M., Babine, R., Li, X., Thacher, S., Hashimoto, H., and Shiozaki, M. (2016) SAR Exploration Guided by LE and Fsp(3): Discovery of a Selective and Orally Efficacious ROR $\gamma$  Inhibitor. *ACS Med Chem Lett* **7**, 23-27
34. Marcotte, D. J., Liu, Y., Little, K., Jones, J. H., Powell, N. A., Wildes, C. P., Silvian, L. F., and Chodaparambil, J. V. (2016) Structural determinant for inducing ROR $\gamma$  specific inverse agonism triggered by a synthetic benzoxazinone ligand. *BMC Struct Biol* **16**, 7
35. Rene, O., Fauber, B. P., Boenig Gde, L., Burton, B., Eidenschenk, C., Everett, C., Gobbi, A., Hymowitz, S. G., Johnson, A. R., Kiefer, J. R., Liimatta, M., Lockey, P., Norman, M., Ouyang, W., Wallweber, H. A., and Wong, H. (2015) Minor Structural Change to Tertiary Sulfonamide ROR $\gamma$  Ligands Led to Opposite Mechanisms of Action. *ACS Med Chem Lett* **6**, 276-281
36. Scheepstra, M., Leysen, S., van Almen, G. C., Miller, J. R., Piesvaux, J., Kutilek, V., van Eenennaam, H., Zhang, H., Barr, K., Nagpal, S., Soisson, S. M., Kornienko, M., Wiley, K., Elsen, N., Sharma, S., Correll, C. C., Trotter, B. W., van der Stelt, M., Oubrie, A., Ottmann, C., Parthasarathy, G., and Brunsveld, L. (2015) Identification of an allosteric binding site for ROR $\gamma$  inhibition. *Nat Commun* **6**, 8833

37. Jencks, W. P. (1981) On the attribution and additivity of binding energies. *Proc Natl Acad Sci U S A* **78**, 4046-4050
38. Knotts, T. A. t., Rathore, N., and de Pablo, J. J. (2008) An entropic perspective of protein stability on surfaces. *Biophys J* **94**, 4473-4483
39. Wang, W., Prosise, W. W., Chen, J., Taremi, S. S., Le, H. V., Madison, V., Cui, X., Thomas, A., Cheng, K. C., and Lesburg, C. A. (2008) Construction and characterization of a fully active PXR/SRC-1 tethered protein with increased stability. *Protein Eng Des Sel* **21**, 425-433
40. Fremont, D. H., Hendrickson, W. A., Marrack, P., and Kappler, J. (1996) Structures of an MHC class II molecule with covalently bound single peptides. *Science* **272**, 1001-1004
41. Reddy Chichili, V. P., Kumar, V., and Sivaraman, J. (2013) Linkers in the structural biology of protein-protein interactions. *Protein Sci* **22**, 153-167
42. Hohenstein, E. G., Chill, S. T., and Sherrill, C. D. (2008) Assessment of the Performance of the M05-2X and M06-2X Exchange-Correlation Functionals for Noncovalent Interactions in Biomolecules. *J Chem Theory Comput* **4**, 1996-2000
43. Zhao, Y., and Truhlar, D. G. (2008) Density functionals with broad applicability in chemistry. *Acc Chem Res* **41**, 157-167
44. Johnson, B. A., Wilson, E. M., Li, Y., Moller, D. E., Smith, R. G., and Zhou, G. (2000) Ligand-induced stabilization of PPARgamma monitored by NMR spectroscopy: implications for nuclear receptor activation. *J Mol Biol* **298**, 187-194
45. Kallenberger, B. C., Love, J. D., Chatterjee, V. K., and Schwabe, J. W. (2003) A dynamic mechanism of nuclear receptor activation and its perturbation in a human disease. *Nat Struct Biol* **10**, 136-140
46. Nolte, R. T., Wisely, G. B., Westin, S., Cobb, J. E., Lambert, M. H., Kurokawa, R., Rosenfeld, M. G., Willson, T. M., Glass, C. K., and Milburn, M. V. (1998) Ligand binding and co-activator assembly of the peroxisome proliferator-activated receptor-gamma. *Nature* **395**, 137-143
47. Eilers, M., Shekar, S. C., Shieh, T., Smith, S. O., and Fleming, P. J. (2000) Internal packing of helical membrane proteins. *Proc Natl Acad Sci U S A* **97**, 5796-5801
48. Edwards, T. A., and Wilson, A. J. (2011) Helix-mediated protein-protein interactions as targets for intervention using foldamers. *Amino Acids* **41**, 743-754
49. Vihinen, M., Torkkila, E., and Riikonen, P. (1994) Accuracy of protein flexibility predictions. *Proteins* **19**, 141-149
50. Parthasarathy, S., and Murthy, M. R. (2000) Protein thermal stability: insights from atomic displacement parameters (B values). *Protein Eng* **13**, 9-13
51. Yuan, Z., Zhao, J., and Wang, Z. X. (2003) Flexibility analysis of enzyme active sites by crystallographic temperature factors. *Protein Eng* **16**, 109-114
52. Fenwick, R. B., van den Bedem, H., Fraser, J. S., and Wright, P. E. (2014) Integrated description of protein dynamics from room-temperature X-ray crystallography and NMR. *Proc Natl Acad Sci U S A* **111**, E445-454
53. Gustafsson, J. A. (2016) Historical overview of nuclear receptors. *J Steroid Biochem Mol Biol* **157**, 3-6
54. Renaud, J. P., and Moras, D. (2000) Structural studies on nuclear receptors. *Cell Mol Life Sci* **57**, 1748-1769
55. Pardee, K. I., Xu, X., Reinking, J., Schuetz, A., Dong, A., Liu, S., Zhang, R., Tiefenbach, J., Lajoie, G., Plotnikov, A. N., Botchkarev, A., Krause, H. M., and Edwards, A. (2009) The structural basis of gas-responsive transcription by the human nuclear hormone receptor REV-ERBbeta. *PLoS Biol* **7**, e43
56. Raghuram, S., Stayrook, K. R., Huang, P., Rogers, P. M., Nosie, A. K., McClure, D. B., Burris, L. L., Khorasanizadeh, S., Burris, T. P., and Rastinejad, F. (2007) Identification of

- heme as the ligand for the orphan nuclear receptors REV-ERB $\alpha$  and REV-ERB $\beta$ . *Nat Struct Mol Biol* **14**, 1207-1213
57. Perissi, V., and Rosenfeld, M. G. (2005) Controlling nuclear receptors: the circular logic of cofactor cycles. *Nature Reviews Molecular Cell Biology* **6**, 542-554
58. Rastinejad, F., Ollendorff, V., and Polikarpov, I. (2015) Nuclear receptor full-length architectures: confronting myth and illusion with high resolution. *Trends Biochem Sci* **40**, 16-24
59. Rastinejad, F., Huang, P., Chandra, V., and Khorasanizadeh, S. (2013) Understanding nuclear receptor form and function using structural biology. *J Mol Endocrinol* **51**, T1-T21
60. Anbalagan, M., Huderson, B., Murphy, L., and Rowan, B. G. (2012) Post-translational modifications of nuclear receptors and human disease. *Nucl Recept Signal* **10**, e001
61. Faus, H., and Haendler, B. (2006) Post-translational modifications of steroid receptors. *Biomed Pharmacother* **60**, 520-528
62. Lim, H. W., Kang, S. G., Ryu, J. K., Schilling, B., Fei, M., Lee, I. S., Kehasse, A., Shirakawa, K., Yokoyama, M., Schnolzer, M., Kasler, H. G., Kwon, H. S., Gibson, B. W., Sato, H., Akassoglou, K., Xiao, C., Littman, D. R., Ott, M., and Verdin, E. (2015) SIRT1 deacetylates ROR $\gamma$  and enhances Th17 cell generation. *J Exp Med* **212**, 607-617
63. Rutz, S., Kayagaki, N., Phung, Q. T., Eidenschenk, C., Noubade, R., Wang, X., Lesch, J., Lu, R., Newton, K., Huang, O. W., Cochran, A. G., Vasser, M., Fauber, B. P., DeVoss, J., Webster, J., Diehl, L., Modrusan, Z., Kirkpatrick, D. S., Lill, J. R., Ouyang, W., and Dixit, V. M. (2015) Deubiquitinase DUBA is a post-translational brake on interleukin-17 production in T cells. *Nature* **518**, 417-421
64. Gallastegui, N., Mackinnon, J. A., Fletterick, R. J., and Estebanez-Perpina, E. (2015) Advances in our structural understanding of orphan nuclear receptors. *Trends Biochem Sci* **40**, 25-35
65. Sablin, E. P., Krylova, I. N., Fletterick, R. J., and Ingraham, H. A. (2003) Structural Basis for Ligand-Independent Activation of the Orphan Nuclear Receptor LRH-1. *Molecular Cell* **11**, 1575-1585
66. Fujioka, M., and Omori, N. (2012) Subtleties in GPCR drug discovery: a medicinal chemistry perspective. *Drug Discov Today* **17**, 1133-1138
67. Manglik, A., Kim, T. H., Masureel, M., Altenbach, C., Yang, Z., Hilger, D., Lerch, M. T., Kobilka, T. S., Thian, F. S., Hubbell, W. L., Prosser, R. S., and Kobilka, B. K. (2015) Structural Insights into the Dynamic Process of beta2-Adrenergic Receptor Signaling. *Cell* **161**, 1101-1111
68. Staus, D. P., Strachan, R. T., Manglik, A., Pani, B., Kahsai, A. W., Kim, T. H., Wingler, L. M., Ahn, S., Chatterjee, A., Masoudi, A., Kruse, A. C., Pardon, E., Steyaert, J., Weis, W. I., Prosser, R. S., Kobilka, B. K., Costa, T., and Lefkowitz, R. J. (2016) Allosteric nanobodies reveal the dynamic range and diverse mechanisms of G-protein-coupled receptor activation. *Nature* **535**, 448-452
69. Pflugrath, J. W. (1999) The finer things in X-ray diffraction data collection. *Acta Crystallogr D Biol Crystallogr* **55**, 1718-1725
70. Kabsch, W. (2010) Xds. *Acta Crystallogr D Biol Crystallogr* **66**, 125-132
71. McCoy, A. J., Grosse-Kunstleve, R. W., Adams, P. D., Winn, M. D., Storoni, L. C., and Read, R. J. (2007) Phaser crystallographic software. *J Appl Crystallogr* **40**, 658-674
72. Adams, P. D., Afonine, P. V., Bunkoczi, G., Chen, V. B., Davis, I. W., Echols, N., Headd, J. J., Hung, L. W., Kapral, G. J., Grosse-Kunstleve, R. W., McCoy, A. J., Moriarty, N. W., Oeffner, R., Read, R. J., Richardson, D. C., Richardson, J. S., Terwilliger, T. C., and Zwart, P. H. (2010) PHENIX: a comprehensive Python-based system for macromolecular structure solution. *Acta Crystallogr D Biol Crystallogr* **66**, 213-221



73. Emsley, P., and Cowtan, K. (2004) Coot: model-building tools for molecular graphics. *Acta Crystallogr D Biol Crystallogr* **60**, 2126-2132
74. Chen, V. B., Arendall, W. B., 3rd, Headd, J. J., Keedy, D. A., Immormino, R. M., Kapral, G. J., Murray, L. W., Richardson, J. S., and Richardson, D. C. (2010) MolProbity: all-atom structure validation for macromolecular crystallography. *Acta Crystallogr D Biol Crystallogr* **66**, 12-21
75. Nietlispach, D. (2005) Suppression of anti-TROSY lines in a sensitivity enhanced gradient selection TROSY scheme. *J Biomol NMR* **31**, 161-166
76. Hwang, T. L., van Zijl, P. C., and Garwood, M. (1997) Broadband adiabatic refocusing without phase distortion. *J Magn Reson* **124**, 250-254
77. Kupce, E., and Freeman, R. (2007) Compensated adiabatic inversion pulses: broadband INEPT and HSQC. *J Magn Reson* **187**, 258-265
78. Kashem, M. A., Nelson, R. M., Yingling, J. D., Pullen, S. S., Prokopowicz, A. S., 3rd, Jones, J. W., Wolak, J. P., Rogers, G. R., Morelock, M. M., Snow, R. J., Homon, C. A., and Jakes, S. (2007) Three mechanistically distinct kinase assays compared: Measurement of intrinsic ATPase activity identified the most comprehensive set of ITK inhibitors. *J Biomol Screen* **12**, 70-83
79. (2006) Jaguar, version 7.9, Schrödinger, LLC, New York, NY, <http://www.schrodinger.com/Jaguar2006>.
80. Zhao, Y., and Truhlar, D. G. (2006) A new local density functional for main-group thermochemistry, transition metal bonding, thermochemical kinetics, and noncovalent interactions. *J Chem Phys* **125**, 194101
81. Tannor, D. J., Marten, B., Murphy, R., Friesner, R. A., Sitkoff, D., Nicholls, A., Honig, B., Ringnalda, M., and Goddard, W. A. (1994) Accurate First Principles Calculation of Molecular Charge Distributions and Solvation Energies from Ab Initio Quantum Mechanics and Continuum Dielectric Theory. *Journal of the American Chemical Society* **116**, 11875-11882

## Footnotes

Unpublished in-house NMR and X-ray data suggest that the C-terminal residues beyond H12 (*i.e.* residues 508 – 518) in the native ROR $\gamma$ t-LBD are largely disordered both in solution and in crystal forms.

**Abbreviations used:** TROSY, transverse relaxation optimized spectroscopy; HSQC, heteronuclear single quantum coherence; Gal4, galactose-responsive transcription factor GAL4; PPAR $\gamma$ , Peroxisome proliferator-activated receptor  $\gamma$  (NR1C3); ESRRG, estrogen-related receptor  $\gamma$  (NR3B3); NGFIB, nerve growth factor IB (NR4A1); NURR1, nuclear receptor related 1 (NR4A2); LRH-1, liver receptor homolog-1 (NR5A2); REV-ERB $\alpha$ , nuclear receptor subfamily 1 group D member 1 (NR1D1); REV-ERB $\beta$ , nuclear receptor subfamily 1 group D member 2 (NR1D2); PDB, Protein Data Bank.

The atomic coordinates and associated structure factors (codes: 5VB3, 5VB5, 5VB6, and 5VB7) have been deposited in the Protein Data Bank (<http://www.wwpdb.org/>).

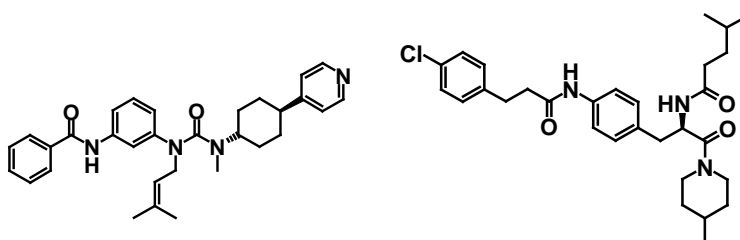
**Table 1****Data collection and structure refinement statistics**

ROR $\gamma$ t LBD	Apo	With Compound 1	With Compound 2	With Compound 3
<b>Data collection</b>				
Wavelength (Å)	1.00	1.00	1.00	1.00
Space group	P4 <sub>1</sub> 2 <sub>1</sub> 2	P4 <sub>1</sub> 2 <sub>1</sub> 2	P4 <sub>1</sub> 2 <sub>1</sub> 2	P4 <sub>1</sub> 2 <sub>1</sub> 2
Unit cell dimensions (a, b, c) (Å)	61.27, 61.27, 154.23	62.31, 62.31, 154.18	60.47, 60.47, 155.00	62.96, 62.96, 155.32
( $\alpha$ , $\beta$ , $\gamma$ ) (°)	90.00, 90.00, 90.00	90.00, 90.00, 90.00	90.00, 90.00, 90.00	90.00, 90.00, 90.00
Mosaicity	0.31	0.19	0.58	0.48
Resolution range (Å)	43.33 - 1.95 (2.02 – 1.95)	77.09 – 2.04 (2.05 – 2.04)	155.00 – 2.23 (2.233 – 2.226)	77.66 – 2.34 (2.342 – 2.335)
Total number of reflections	258813	261150	182584	175314
Number of unique reflections	21942	20213	14904	14031
Average redundancy	11.80 (12.56)	12.9 (12.6)	12.3 (11.9)	12.5 (13.3)
Completeness (%)	98.5 (98.0)	100.0 (100.0)	100.0 (100.0)	100.0 (100.0)
R <sub>merge</sub>	0.074 (0.593)	0.086 (1.202)	0.099 (1.490)	0.114 (1.903)
R <sub>meas</sub>	0.078 (0.618)	0.090 (1.254)	0.104 (1.558)	0.119 (1.978)
Output <I/ $\sigma$ <sub>I</sub> >	14.4 (3.2)	25.0 (2.2)	15.4 (2.4)	18.9 (2.4)
<b>Refinement</b>				
Resolution range (Å)	43.33 – 1.95	39.65 – 2.04	39.28 – 2.23	38.62 – 2.34
Reflections, Work/Test (%)	21934/1123 (5.12%)	20131/1002 (4.98%)	14824/739 (4.99%)	13954/704 (5.05%)
Completeness for range (%)	98.82	99.95	99.85	99.89
Number of atoms	2300	2346	2268	2215
Number of waters	159	190	102	80
R <sub>work</sub>	0.1957	0.1866	0.1932	0.1836
R <sub>free</sub>	0.2298	0.2075	0.2344	0.2161
Rmsd bond lengths (Å)	0.004	0.003	0.002	0.005
Rmsd bond angles (°)	0.731	0.621	0.534	0.600
Average B value (Å <sup>2</sup> )	36.62	33.79	45.54	42.07
<b>Ramachandran Plot</b>				
Favored (%)	98.85	97.72	98.85	98.45
Allowed (%)	1.15	2.28	1.15	1.55
Outliers (%)	0.0	0.00	0.00	0.00

Note: Values in ( ) are for the last resolution shell.

**Table 2**

**Inverse agonists of ROR $\gamma$ t reported in this study**



	<b>Compound 1</b>	<b>Compound 2</b>
ROR $\gamma$ t Binding $K_d$ ( $\mu$ M)	$0.43 \pm 0.18$	$0.35 \pm 0.22$
ROR $\gamma$ t RGA $IC_{50}$ ( $\mu$ M)	$0.64 \pm 0.12$	$0.56 \pm 0.15$
Th17 $IC_{50}$ ( $\mu$ M)	$0.9 \pm 0.8$	$1.5 \pm 0.6$

## Figure legends

**Figure 1.** Apo structure of ROR $\gamma$ t ligand binding domain (LBD) and structural determinants for its active conformation. A, schematic representation of the apo ROR $\gamma$ t LBD is shown in pale green, with H11', H12 and SRC2 peptide segments highlighted in green, dark red and xenon blue, respectively. The large cavity present in the apo ROR $\gamma$ t is shown in dark grey. His323, His479, Tyr502 and Phe506 are highlighted as sticks. B, superposition of the apo ROR $\gamma$ t structure in dark red with the ROR $\gamma$ t LBD bound with 25-hydroxycholesterol (25-HC) in light grey (PDB ID: 3L0L); 25-HC is drawn as green sticks. Close-up views are shown for the SRC2 peptide and H12 regions and for the apo state cavity with 25-HC and H323, H479, Y502 and F506 highlighted. The B-ring of 25-HC protrudes out of the apo cavity and would clash with the sidechain of H323 in the apo state. C, close interactions among the H479-Y502-F506 triplet in ROR $\gamma$ t help to anchor Helix12 in the active conformation. Color scheme follows that of Figure 1A. The H-bond between H479 and Y502 is indicated as black dashes. D, helical packing between H11', H12 and the SRC2 peptide provides further stabilization. The solvent accessible surface areas of the three helical elements are depicted as meshes and highlighted in a close-up view. Color scheme follows that of Figure 1A.

**Figure 2.** NMR spectra of ROR $\gamma$ t(259-518) and ROR $\gamma$ t(260-507)-G<sub>3</sub>-SRC2. A, B: Overlays of backbone <sup>15</sup>N-TROSY (A) and methyl <sup>13</sup>C-HSQC (B) spectra of ROR $\gamma$ t(259-518) in apo (black) and in SRC2 peptide bound state (red). Some perturbed peaks are highlighted with green arrows. C, D: Overlays of backbone <sup>15</sup>N-TROSY (C) and methyl <sup>13</sup>C-HSQC (D) spectra of ROR $\gamma$ t(260-507)-G<sub>3</sub>-SRC2 (blue) and SRC2 peptide bound ROR $\gamma$ t(259-518) (red). The methyl peaks highlighted in Figure 3B are indicated with the same green arrows in Figure 3D.

**Figure 3.** Binding modes of Compounds **1**, **2** and **3**. Compounds are shown in magenta in the ligand binding pocket of ROR $\gamma$ t of the respective co-complex structures. The overall structures of ligand-bound ROR $\gamma$ t LBD are depicted in cartoons, with H11', H12 and SRC2 peptide colored as in Figure 1A and key ligand binding site residues highlighted as sticks. The simulated annealing omit difference maps were calculated with the entire compound molecules omitted, and plotted in blue at 2.5  $\sigma$  level for Compounds **1** and **2**, and at 3.0  $\sigma$  level for Compound **3**. The apo structure of ROR $\gamma$ t is shown in pale green as in Figure 1A. Compounds are shown in magenta sticks. H-bonds are indicated as black dashes. A, the overall binding mode of Compound **1**. B, close-up view of Compound **1**'s disruption to the H479-Y502-F506 triplet in ROR $\gamma$ t. C, the overall binding mode of Compound **2**. D, close-up view of Compound **2**'s disruption to the H479-Y502-F506 triplet in ROR $\gamma$ t. E, the overall binding mode of Compound **3**. F, a cluster of aryl interactions are formed between Compound **3**, the H479-Y502-F506 triplet and Trp317 which further stabilize ROR $\gamma$ t in the active conformation. Compound **1** and His479 from Compound **1**-bound ROR $\gamma$ t are shown in yellow for comparison; only protein atoms were used in the superposition.

**Figure 4.** Differential B-factor plot. Normalized B-factor differences (see main text) are displayed for the structural elements as a blue-white-red color ramp with blue indicating the most negative value (stabilization) and red the most positive value (destabilization). The compound chemical structure is drawn at the top of each respective panel. A, for H11 and H12 of ROR $\gamma$ t in complex with Compound **1**. B, for H11 and H12 of ROR $\gamma$ t in complex with Compound **2**. C, for H11 and H12 of ROR $\gamma$ t in complex with Compound **3**.



**Figure 5.** Agonistic effect of Compound **3** as shown in the FP based coactivator recruitment assay. The compound concentration is plotted in logarithmic scale.

**Figure 1**

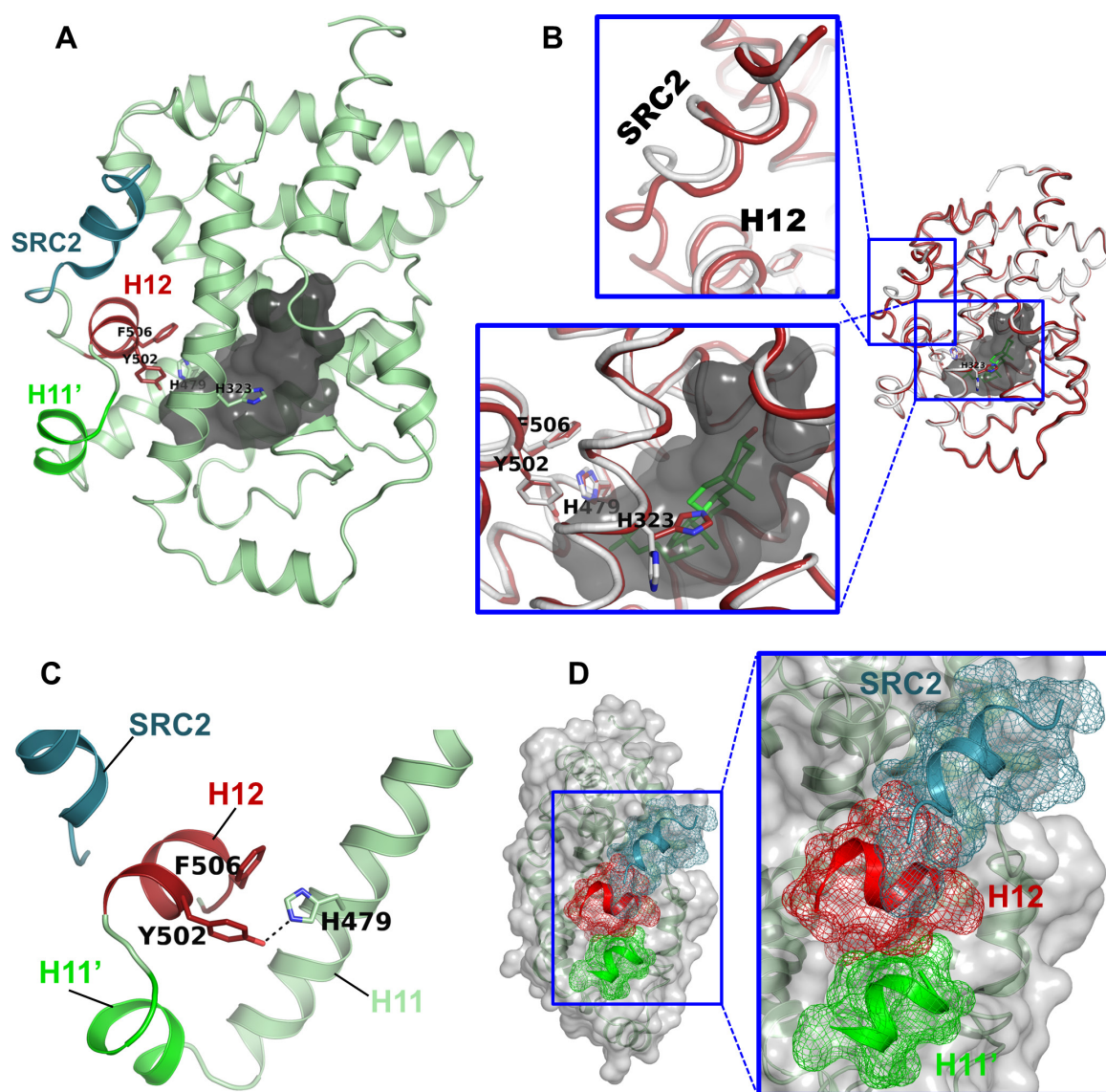


**Figure 2**

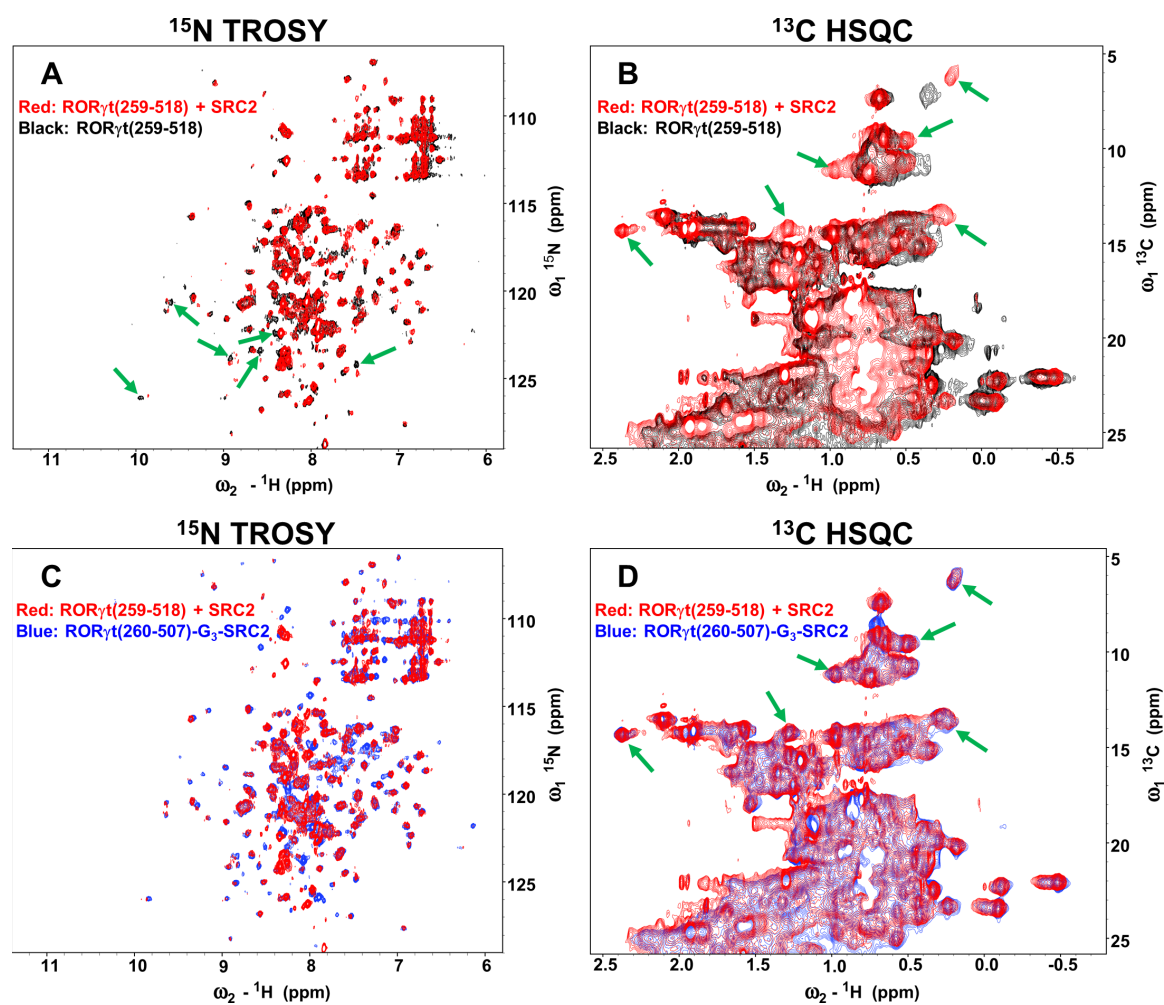


**Figure 3**

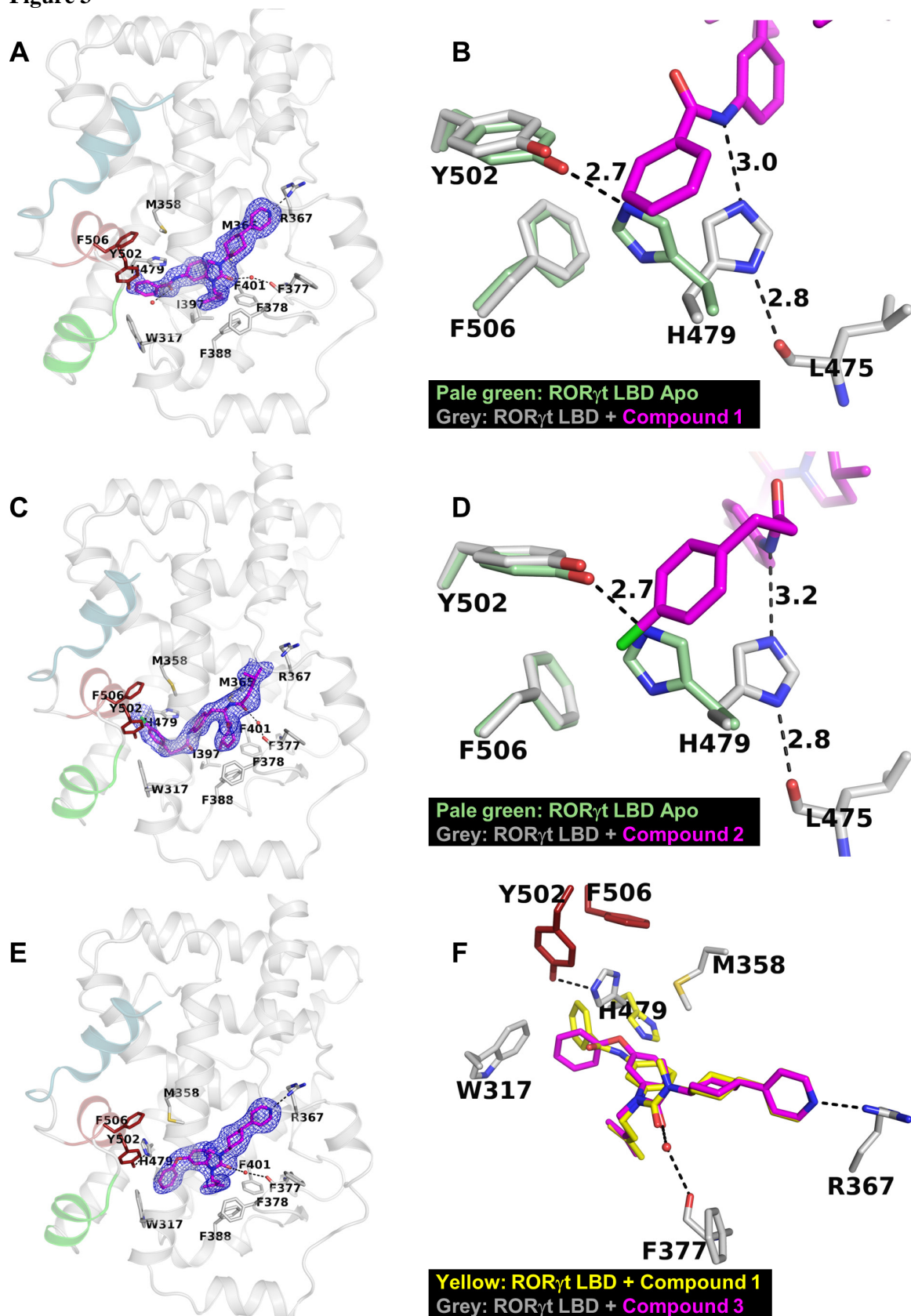




**Figure 4**

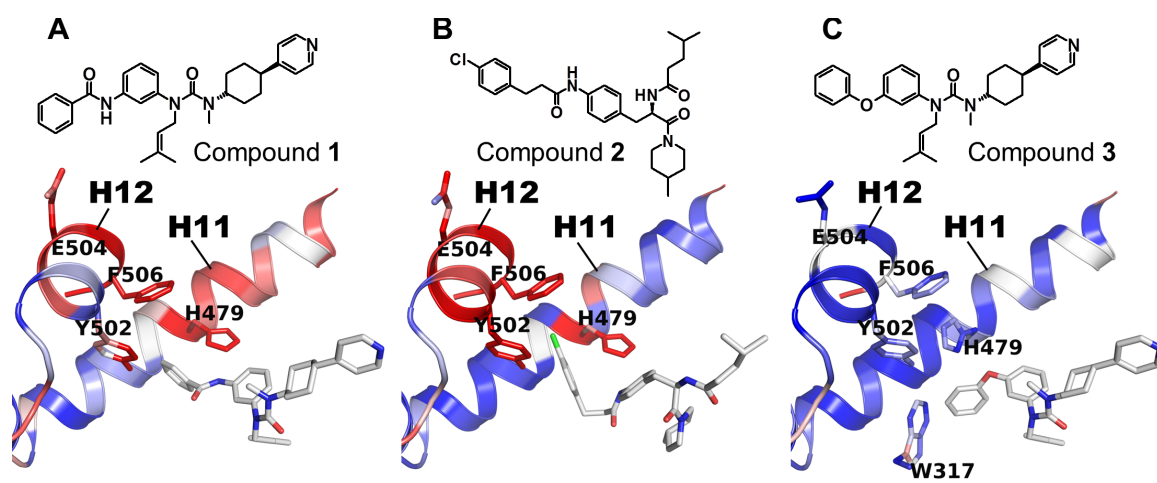
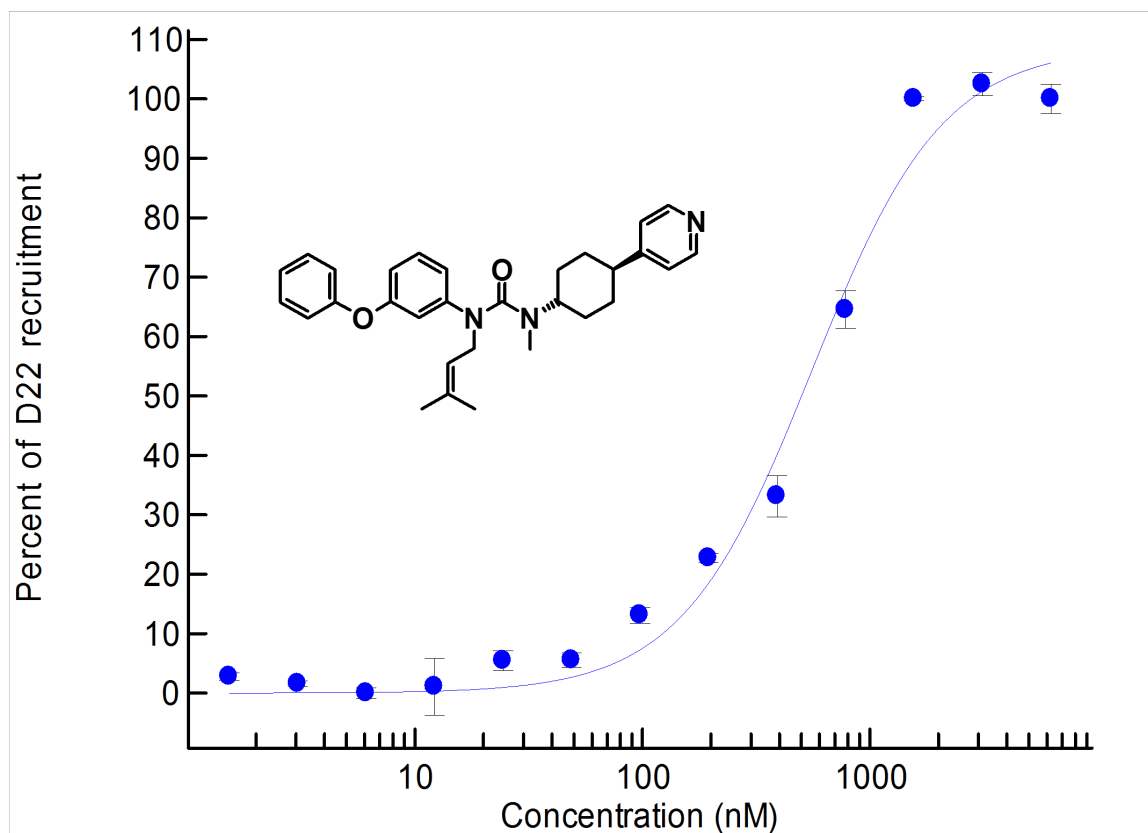


**Figure 5**



**Structural studies unravel the active conformation of apo ROR $\gamma$  nuclear receptor and a common inverse agonism of two diverse classes of ROR  $\gamma$  inhibitors**

Xiang Li, Marie Anderson, Delphine Collin, Ingo Muegge, John Wan, Debra Brennan, Stanley Kugler, Donna Terenzio, Charles Kennedy, Siqu Lin, Mark E. Labadia, Brian Cook, Robert Hughes and Neil A. Farrow

*J. Biol. Chem.* published online May 25, 2017

---

Access the most updated version of this article at doi: [10.1074/jbc.M117.789024](https://doi.org/10.1074/jbc.M117.789024)

Alerts:

- [When this article is cited](#)
- [When a correction for this article is posted](#)

[Click here](#) to choose from all of JBC's e-mail alerts

Supplemental material:

<http://www.jbc.org/content/suppl/2017/05/25/M117.789024.DC1>

This article cites 0 references, 0 of which can be accessed free at

<http://www.jbc.org/content/early/2017/05/25/jbc.M117.789024.full.html#ref-list-1>